Title	Photochromism and Long Persistent Luminescence in Pr^<3+>-Doped Garnet Transparent Ceramic via Ultraviolet or Blue Light Up-conversion Charging
Author(s)	Du, Qiping; Ueda, Jumpei; Zheng, Ruilin; Tanabe, Setsuhisa
Citation	Advanced Optical Materials, 11(7): 2202612
Issue Date	2023-01-19
Type	Journal Article
Text version	author
URL	http://hdl.handle.net/10119/18800
Rights	This is the peer reviewed version of the following article: Qiping Du, Jumpei Ueda, Ruilin Zheng, and Setsuhisa Tanabe, Advanced Optical Materials, 11, 7, 2202612 (2023), which has been published in final form at https://doi.org/10.1002/adom.202202612. This article may be used for non-commercial purposes in accordance with Wiley Terms and Conditions for Use of Self-Archived Versions. This article may not be enhanced, enriched or otherwise transformed into a derivative work, without express permission from Wiley or by statutory rights under applicable legislation. Copyright notices must not be removed, obscured or modified. The article must be linked to Wiley's version of record on Wiley Online Library and any embedding, framing or otherwise making available the article or pages thereof by third parties from platforms, services and websites other than Wiley Online Library must be prohibited.
Description	

Photochromism and Long Persistent Luminescence in Pr^{3+}-Doped Garnet Transparent Ceramic via Ultraviolet or Blue Light Up-conversion Charging

Qiping Du[*], Jumpei Ueda[*], Ruilin Zheng, and Setsuhisa Tanabe

Qiping Du, Jumpei Ueda, Ruiling Zheng, and Setsuhisa Tanabe
Graduated School of Human and Environmental Studies, Kyoto University, Kyoto, 6068301, Japan
E-mail: du.qiping.18p@st.kyoto-u.ac.jp

Jumpei Ueda
Graduate School of Advanced Science and Technology, Japan Advanced Institute of Science and Technology, Ishikawa 923-1292, Japan
E-mail: ueda-j@jaist.ac.jp

Abstract: Multifunctional phosphors with photochromism and persistent luminescent (PersL) properties have attracted increasing interest owing to the capability of absorbing the photon energy and trapping the generated carriers via defects. However, the opacity of materials compromises the enhancement of photochromism and PersL properties; besides, the need of high energy excitation light source limits their applicability. To bridge these obstacles, we report Pr^{3+}-doped Y$_3$Al$_2$Ga$_3$O$_{12}$ transparent ceramic with in-line transmittance over 80% at 1800 nm, which exhibits strong red PersL after several minutes ultraviolet (UV) light or blue light up-conversion charging. The luminance duration time can reach more than 7 h at 0.32 mcd /m^2 threshold value after UV light charging. Interestingly, the phosphor also displays photochromic properties with robust fatigue resistance, i.e., the color changes from light green to red by UV/blue light illumination and is bleached at 300°C. The nature of trap centers, trapping and detrapping processes are explored based on thermoluminescence and electron spin resonance. Finally, the mechanism of photochromism and PersL are discussed by using vacuum referred binding energy diagram. This work opens new avenues for future research on multifunctional materials and brings potential applications in optical information encryption media and optical sensors.

1. Introduction

On the basis of an unprecedented explosion of the total mass amount of digital information data, information storage has received increasing attention.[1] Growing endeavors have been made to develop sustainable and versatile optical data storage and conversion materials due to their advantages, i.e., high storage density, long lifetime, easy portability, and exceptional rewritability in recent years.[2] Photochromism is the phenomenon that the material changes its color by the illumination of light.[3] In these materials, the information can effectively be written optically and returned to the original state by stimulation of an external field, such as heat, light illumination, or mechanical stress.[4] Organic photochromic materials (i.e., azobenzenes,[5] spiropyrans,[6] naphthopyrans,[7] and diarylethenes[8]) have been widely studied. Compared with organic photochromic counterparts, controllable macroscopic shape molding, chemical fatigue resistance, high thermal stability and mechanical strength of inorganic photochromic materials can enhance their applicability. To date, a series of inorganic photochromic materials have been extensively explored, including transition metal oxides (WO_3,[9] TiO_2[10] and MoO_3[11]), ferroelectric ceramics ($Na_{0.5}Bi_{2.5}Nb_2O_9$,[12] $Na_{0.5}Bi_{0.5}TiO_3$[13] and $K_{0.5}Na_{0.5}NbO_3$[14]) and robust oxides ($BaMgSiO_4$,[15] $PbWO_4:Yb^{3+}$, Er^{3+},[16] and Sr_2SnO_4[17])). Taking advantage of their photochromism and reversible luminescence modulation properties, these materials could be used in optical data storage applications. Persistent Luminescence (PersL) materials and thermoluminescence materials also belong to another specific member of the family applied in optical information storage devices.[18] PersL materials can store the photon energy under exposure of short-wavelength electromagnetic waves, and last luminescence for a long time after ceasing the excitation light source. Traps are responsible for the photon storage (trapping) and release (detrapping) in the PersL materials. Also, the probability of charge carries detrapping are largely affected by the trap depth and activation energy. The well-known green-emitting $SrAl_2O_4$: Eu, Dy PersL phosphor was described by Matsuzawa et al in the literature in

1996, which possesses large amounts of traps with 0.5-0.8 eV depth and is applied in night-vision security signs.[19]

Since then, many new PersL phosphors with emissions spanning from the ultraviolet (UV) to the near-infrared (NIR) have been developed. In terms of green or blue PersL phosphors, [20]these materials show intense luminescence and long PersL duration time (more than 10h), while reports on high-performance PersL phosphors with red emission at 600-650 nm are so far still scarce in the literature. For this reason, one of the main topics of research in this area involves improving these red PersL properties through the implementation of activating ions. Phosphors such as Y_2O_2S: Eu^{3+}, Mg^{2+}, Ti^{4+}[21] and CaS: Eu^{2+}, Tm^{3+}[22] exhibit the red PersL, however, they have poor chemical stability and a relatively short PersL duration time. Within the last few years, other phosphors such as Sr_3SiO_5: Eu^{2+}, Dy^{3+},[23] $Ca_2Sr_2Si_5N_8$: Eu^{2+},[24] $CaAlSiN_3$: Eu^{2+},[25] and $Ca_3Ti_2O_7$: Pr^{3+}[26] have been reported, while the duration time was still not so long. Besides, in most cases, the occurrence of PersL requires high excitation energy, usually UV light from mercury lamps or xenon arc lamps. For wide applications, it is desirable to use low-energy photons to achieve effective charging. Up-conversion charging can be a more promising way to promote the luminescence ion system to a high-energy delocalized state by low energy photon excitation, followed by filling traps in the materials.[27] Pan et al. reported that Cr^{3+} doped $Zn_3Ga_2GeO_8$ compound was added with the Er^{3+}-Yb^{3+} up-conversion ion pair. The combination of up-conversion charging and PersL can overcome the drawbacks in the bio-imaging field application.[28] Also, instead of commonly opaque PersL phosphors such as pellet or powder, transparent ceramic phosphors with high density and optical transparency performed stronger PersL because they can be illuminated within the whole body, which induces the carrier formation inside the sample by taking the advantages of lower optical scattering coefficient.[29]

To date, phosphors showing both photochromism and PersL have been reported following the strong demand for novel smart optical storage materials, however, these materials are

opaque and commonly charged by high energy light.[30] Herein, we aim at developing a novel multifunctional transparent ceramic which should fulfill the following criteria: (1) high transparency (2) red PersL and long duration time (3) low energy blue light excitation via up-conversion charging (4) reversible photochromism property. Firstly, optical transparent ceramics generally need to have an isotropic lattice structure (such as a cubic structure). Garnet structure represented by the most famous $Y_3Al_5O_{12}$ (YAG) host in the form of $A_3[B]_2(C)_3O_{12}$ is belonging to the cubic crystal system with a space group of *Ia3d*. Three cation sites A, [B], and (C) represent cations that occupy the dodecahedral, octahedral, and tetrahedral sites, respectively. We reported a series of novel garnet persistent phosphors with a host of $Y_3Al_{5-x}Ga_xO_{12}$ co-doped with rare earth luminescent ions or transition metal ions, especially for the transparent ceramic phosphor with the composition of $Y_3Al_2Ga_3O_{12}$ (YAGG): Ce^{3+} (0.2%)-Yb^{3+}(0.1%), which exhibits the PersL for over 138.8 h.[29] Thus, YAGG can be served as an excellent candidate for PersL. Secondly, a suitable trap for all commercial PersL phosphors is a vital condition to obtain high PersL performance. Dorenbos proposed vacuum referred binding energy (VRBE) diagrams and it was successfully applied to predict the energy levels of lanthanide ions in many materials.[31] With the knowledge of the VRBE diagram of the YAGG (Ga = 3) host (energy level), we assume that Pr^{3+} is the most effective ion for achieving red PersL and can be charged by the up-conversion process due to the following attributes: (1) the $^3P_0$ or $^1D_2$ level of Pr^{3+} may play the role of an intermediate state in the up-conversion charging process.[32] (2) the ground state of Pr^{3+} ($^3H_4$) is located above the top of the valence band (VB) with 1.78 eV large energy gaps, giving rise to a stable recombination center. (3) red emission from the $^1D_2$ energy level. Considering the innate advantages of Pr^{3+}, we chose Pr^{3+} as the appropriate activator.

As expected, we successfully developed a multifunctional transparent ceramic phosphor of Pr^{3+}-doped $Y_3Al_2Ga_3O_{12}$ with in-line transmittance over 80% at 1800 nm for the first time. The phosphor exhibits both photochromism and strong red persistent luminescence after several

minutes UV light charging or blue light up-conversion charging. The color of the sample changes to reddish after UV/blue light irradiation and can be recovered by heat treatment. The sample displays strong red PersL and a long luminance duration time of more than 7 h by 5 min UV light charging. Employing a series of optical characterizations combined with the electron spin resonance measurement, its photochromism property, long PersL property, and trapping-detrapping mechanism can be investigated.

2. Results and Discussion

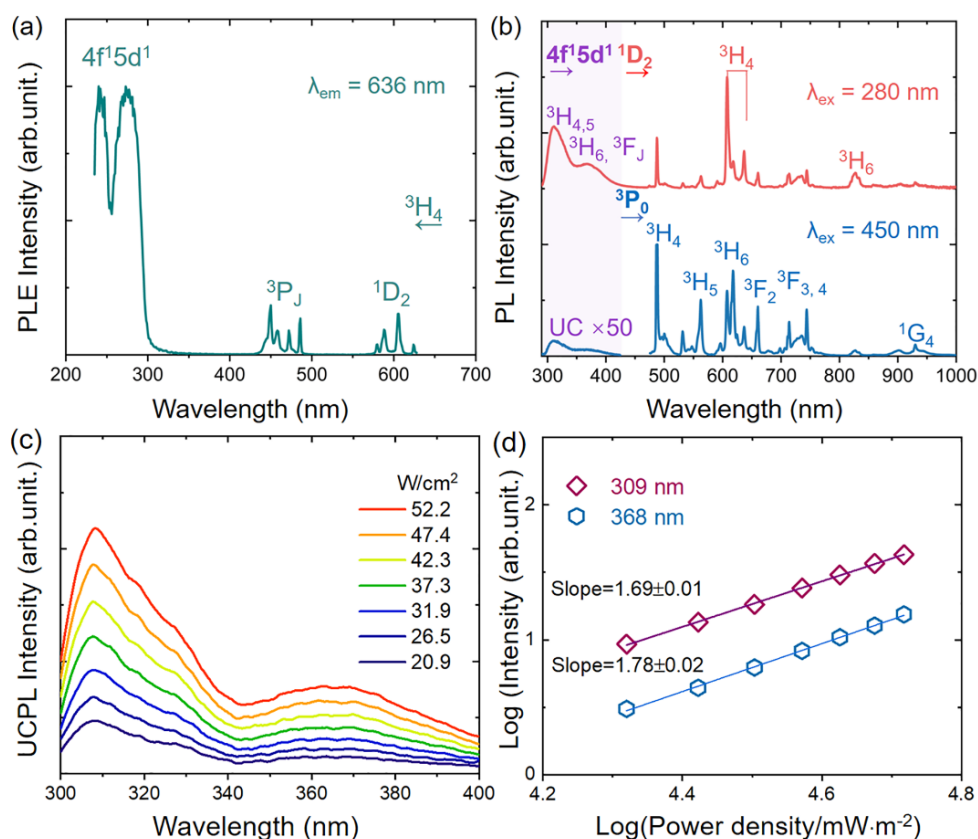### 2.1 Photoluminescence Properties of YAGG: Pr³⁺ Transparent Ceramic

Figure 1. a) PLE spectrum and b) PL spectra of the YAGG: Pr³⁺ transparent ceramic under 280 and 450 nm light excitation. c) Up-conversion Photoluminescence (UCPL) spectra of the YAGG: Pr³⁺ transparent ceramic under various pump power densities from 20.9 to 52.2 W cm⁻² of 450 nm laser excitation. d) Log-Log scale of UCPL intensities monitoring 309 and 368 nm vs. pumping power density.

Figure 1a presents the photoluminescence excitation (PLE) spectrum of the YAGG: Pr³⁺ transparent ceramic sample monitoring the $^1D_2 \rightarrow {}^3H_4$ emission at 636nm. The broad band located in the UV spectral region with a maximum peak at 280 nm corresponds to the transition

from the $^3H_4$ ground state to the lowest $5d_1$ level of Pr^{3+}. The several narrow peaks located in the spectral range of 400-500 nm and 560-630 nm are assigned to the $^3P_J \leftarrow {^3H_4}$, $^1D_2 \leftarrow {^3H_4}$ transitions, respectively. The normalized emission spectra under different excitation wavelengths (λ_{ex} = 280 and 450 nm) of YAGG: Pr^{3+} transparent ceramic are presented in Figure 1b. When the sample is excited by 280 nm light, two strong emission bands distributed in the UV spectral region with the maxima at 312 nm and 368 nm are ascribed to the broad, parity allowed $4f^15d^1 \rightarrow 4f^2$ interconfigurational transitions of Pr^{3+} ion. Several relatively 4f-4f transition emission peaks at 487, 533, 562, 660, 714, 745, 827, and 932 nm can be attributed to $^3P_0 \rightarrow {^3H_4}$, $^3P_1 \rightarrow {^3H_5}$, $^3P_0 \rightarrow {^3H_5}$, $^3P_0 \rightarrow {^3F_2}$, $^3P_0 \rightarrow {^3F_3}$, $^3P_0 \rightarrow {^3F_4}$, $^1D_2 \rightarrow {^3H_6}$, and $^3P_0 \rightarrow {^1G_4}$ transitions, respectively. In addition, the emission peak from 607 to 617 nm derives from the overlap of $^3P_0 \rightarrow {^3H_6}$ and $^1D_2 \rightarrow {^3H_4}$ transitions. Under the excitation of 450 nm (into $^3P_2$), the emission spectrum of the sample is shown in Figure 1b (blue line). Emissions originated from $^3P_0$ level (peak at 487, 562, 617, 660, 714, 745, and 932 nm) are enhanced compared with excitation of 280 nm. Apart from the spectra lines in the visible region due to 4f-4f transitions, two UV emission bands from 300 nm to 430 nm also can be obtained. In the case of 280 nm excitation, the occurrence of the broad UV emission indicates that the lowest energy component of the $4f^15d^1$ configuration is located below the $^1S_0$ state of Pr^{3+}. It is worth noting that the main contribution to the 4f-4f emission is from the $^1D_2$ state to the ground state of the Pr^{3+} ions and the energy allocated to the ^3P_J state is not dominant. Upon excitation with 450 nm, the relative intensity of emission originated from the $^3P_0$ level becomes stronger. As is known, the $^3P_0$ level can be depopulated non-radiatively through a $^3P_0 \rightarrow {^1D_2}$ multiphonon relaxation process and/or through cross relaxation process. The energy gap between the $^3P_0$ and $^1D_2$ levels is around 3300-3400 cm^{-1}, and the phonon energy of YAGG is similar to 820 cm^{-1} of $Y_3Al_5O_{12}$ (YAG). Thus, at least four high energy phonons are required to bridge the gap between the $^3P_0$ and $^1D_2$ levels.[33] Concurrently, the cross relaxation is suppressed by a lower concentration of the Pr^{3+}

ion. Therefore, PL spectrum shows a quite intense emission from $^3P_0$ state under 450 nm excitation (upon ^3P_J state), while 280 nm excitation (upon $4f^1 5d^1$ state) has a direct sensitization process to $^1D_2$ level, which may be caused by a low-lying 4f5d configuration of Pr^{3+}.[34]

To clarify the up-conversion process involved in UV emission under blue light excitation, the dependence of the emission intensity on the pump power density of 450 nm CW laser varying from 20.9-52.2 W cm^{-2} is investigated in Figure 1c. The number of photons required to populate the upper emitting levels can be well obtained by the following equation:

$$I_{UC} \, \alpha \, P^n \tag{1}$$

where I_{UC} is the up-conversion emission intensity, P is the pump power of excitation light, and n is approximately equal to the number of pump photons required to the upper emitting levels. Figure 1d displays a plot of pump power versus emission intensity in double logarithmic scales. The slopes n for 309 and 368 nm from $4f^1 5d^1$ emission are estimated to be 1.69 and 1.78, suggesting that the UV emissions are two-photon excitation processes. The up-conversion emission in the UV region may be due to the excited state absorption (ESA) of Pr^{3+} ion. [35] The Pr^{3+} ion may first be excited to $^3P_2$ level using intense blue light and then relaxes rapidly to an intermediate state (i.e., $^3P_0$). The intermediate-state electron may be further promoted to the Pr^{3+} $4f^1 5d^1$ level and emit UV light. Meanwhile, the pump power density dependence of PL spectra in the 470 to 1000 nm region, and the Log-Log scale of PL intensities monitoring 487 (from $^3P_0$ state) and 607 nm (from $^1D_2$ state) are shown in Figure S1a and S1b (Supporting information), the slope n for the emission at 487 and 617 nm are 0.82, indicating a linear dependence on the laser intensity.

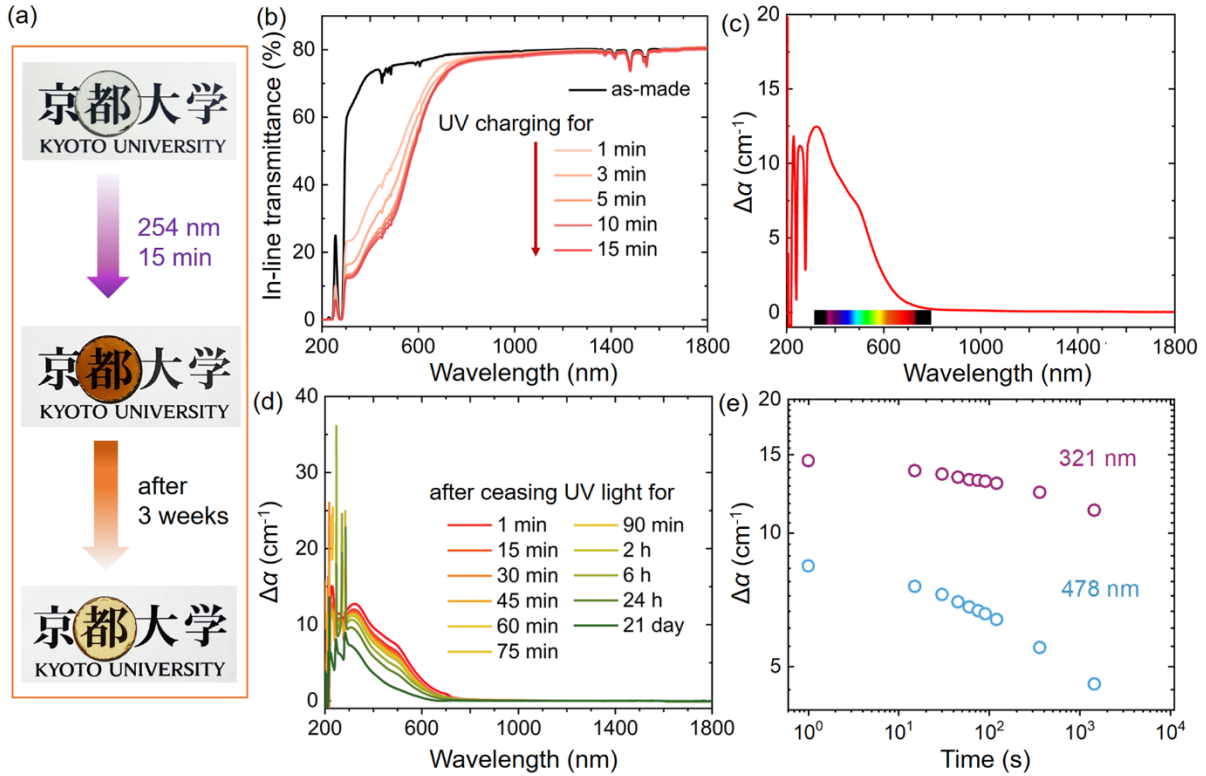## 2.2 Photochromism in YAGG: Pr^{3+} Transparent Ceramic

Figure 2. a) Photographs of the YAGG: Pr^{3+} transparent ceramic sample before (upper) and after (middle) UV(λex = 254 nm) light charging for 15 min. The bottom photograph of the sample shows decoloration after ceasing the UV light after 3 weeks. b) Variation of in-line transmittance spectra of as-made YAGG: Pr^{3+} transparent ceramic during the charging process by 254 nm mercury lamp with different charging times. c) Difference of absorption coefficient ($\Delta\alpha$) spectra after and before UV charging. d) Time-dependence of $\Delta\alpha$ spectra after ceasing UV light with different duration time. e) Time-dependence of $\Delta\alpha$ monitoring at 321 and 478 nm in log-log scale.

A worth noticing phenomenon was the fascinating photochromism of the YAGG: Pr^{3+} transparent ceramic. The greenish color of the sample has turned to reddish color after excitation by the UV light. This photochromism phenomenon was investigated by recording the in-line transmittance spectra of the YAGG: Pr^{3+} transparent ceramic before and after 254 nm UV light charging, as shown in **Figure 2**a. The as-made sample exhibits high transparency, which is over 80% transmittance at 1800 nm. For the as-made sample without UV charging, a strong absorption band appears in the range of 230-350 nm, which is attributed to the 5d $\leftarrow$ 4f transition of the Pr^{3+} ions. Several sharp absorption lines in the visible region are ascribed to the ^3P_J, $^1I_6 \leftarrow {}^3H_4$ (420-500 nm), and $^1D_2 \leftarrow {}^3H_4$ (580-630 nm) transitions, respectively. The sharp absorption lines in the NIR region at around 1300 nm are assigned to the transitions from $^3H_4$

8

to $^3F_{3,4}$ of Pr^{3+}. With continuing to charge the sample with UV light, additional intense absorption bands in the UV/visible spectral regions can be observed, resulting in the reddish color change of the YAGG: Pr^{3+} transparent ceramic. In addition, the absorption intensity became stronger with increasing charging time. The absorption band of the photochromic center was found to be broad in the visible range. To further clarify the photochromism phenomenon in the sample, the absorption coefficient of the sample has been presented as a function of wavelength using the equation:

$$\alpha = \frac{1}{d}\ln\left(\frac{1}{T}\right) \tag{2}$$

where d is the thickness of the sample and T is the transmittance. The absorption coefficient spectra of the sample before and after UV charging are shown in Figure S2 (Supporting Information). Figure 2c presents the difference of absorption coefficient spectra ($\Delta\alpha = \alpha_{after}$ - α_{before}), which can be used to monitor the absorption of photochromic centers. The $\Delta\alpha$ spectrum shows a broad absorption tail in the UV/visible range with two apparent band peaks around 321 and 478 nm responsible for the color change of the sample (deconvolution with Gaussian function of the $\Delta\alpha$ spectrum is provided in Figure S3 (Supporting Information)). To avoid the formation of photochromic centers from other aspects, non-doped sample were fabricated to compare. The in-line transmittance spectra of non-doped YAGG transparent ceramic before and after UV light charging are supplemented in Figure S4a (Supporting Information). For the as-made non-doped sample, no absorption peaks appear in the visible region of the spectrum. However, strong absorption bands in the UV/visible region can be observed after 5 min UV light charging. Comparing with the Pr^{3+}-doped and non-doped YAGG transparent ceramics of $\Delta\alpha$ spectra, similar absorption bands prove that the photochromic centers exist in the YAGG lattice (Figure S4b, Supporting Information). The time-dependence of $\Delta\alpha$ measurements after UV light stoppage was used to reveal variations within detrapping process. Figure 2d presents the evolution of $\Delta\alpha$ converted by transmittance (Figure S5, Supporting Information) after UV

charging for 5 min as a function of duration time at room temperature. With increasing the duration time from 1 min to 3 weeks, the intensity of Δα decreases. In the detrapping process, the colored sample gradually recovers to its initial state at room temperature. It is worth noting that the Δα spectrum still shows a broad absorption tail in the UV/visible range when the duration time is 3 weeks, and the bottom photograph of the sample in Figure 2a also can demonstrate this result. Additionally, to clarify the photochromic centers created after UV irradiation, time-dependence of Δα monitoring at 321 and 478 nm in the Log-Log scale are shown in Figure 2e. Although the intensities of Δα of two photochromic centers decrease with increasing duration time, two absorption decay curves within the detrapping process show a different tendency. For the absorption decay curve of the photochromic center at 321 nm, the slope gives a much more gentle tendency compared with the photochromic center peak at 478 nm. The results suggest two photochromic centers exist, which have different trap depths.

The coloration contrast is also an essential parameter for photochromic materials, which can be presented by the transmittance contrast degree (ΔR_t).[36] The ΔR_t of the YAGG: Pr^{3+} transparent ceramic located at 321 nm is expressed by the formula:

$$\Delta R_t = \frac{T_0 - T_i}{T_0} \times 100\% \tag{3}$$

where the T_0 is the initial transmittance of as-made sample and the T_i is the transmittance of the sample illuminated for different charging times with UV light. As the charging time increased from 1 to 3, 5, 10 and 15 minutes, the calculated ΔR_t reached 63.4%, 72.5%, 80.0%, 80.2 % and 80.5%, respectively. A saturated transmittance contrast degree of 80% was obtained after UV light charging for 5 min. Compared with previous transparent inorganic multifunctional materials,[30] the remarkably large coloration contrast in the YAGG: Pr^{3+} transparent ceramic exhibits remarkable photochromic property.

This photochromism induces an increase in the material absorption in the UV/visible range. An evolution of the PL emission intensity can therefore be expected. Figure S6 (Supporting

Information) presents the evolution of the PL spectra before and after UV charging with different excitation time. As increasing the charging time, a rise of the PL intensity of $^1D_2 \rightarrow$ $^3H_4$ emission (607 nm) is observed, however, the emission from ^3P_J luminescence appears to become weak gradually (from 2 min). After 5 min charging, $^3P_0 \rightarrow ^3H_4$ emission (487 nm) attenuation is reached with a loss of about 15% of the initial intensity; $^1D_2 \rightarrow ^3H_4$ emission (607 nm) is increased by 2 times of the initial intensity. This decrease in the PL intensity is unexpected in PersL materials, in which a gradual increase in the PL emission with time is more likely to occur.[36] Thus, this decrease in PL intensity of ^3P_J emission is possibly linked to the photochromic center, through which the energy transfer from the $^3P_0$ to $^1D_2$ may exist as well.
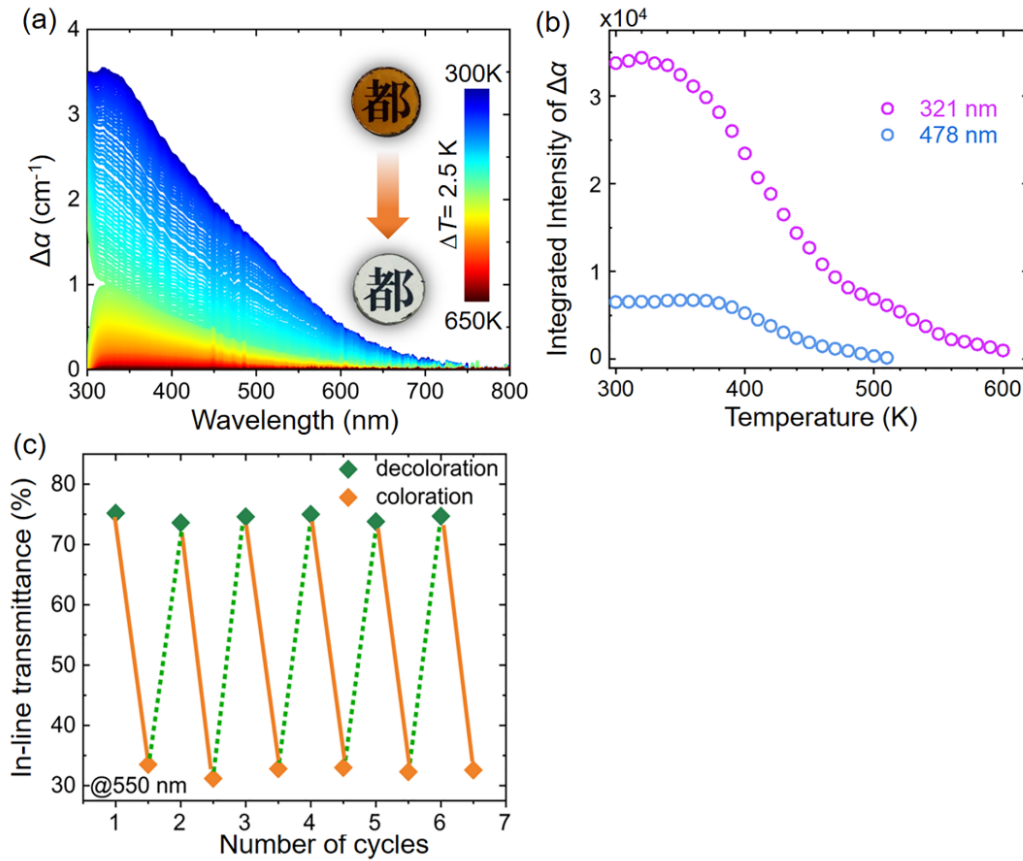

Figure 3. a) Variation of Δα spectra of as-made YAGG: Pr^{3+} transparent ceramic during detrapping process from 300K to 650K with a heating rate of 5K min^{-1}. b) Integrated absorption intensity of Δα monitoring at 321 and 478 nm from spectra in figure 3a per 10K at each point as a function of temperature (300-650 K). c) in-line transmittance of the sample at 550 nm by alternating between UV irradiation and heating at 300℃ for 5 min as a function of cycle numbers.

11

In-situ temperature-dependence of $\Delta\alpha$ can be a good indicator to discuss the thermally detrapping behavior of the YAGG: Pr^{3+} transparent ceramic. $\Delta\alpha$ spectra against the temperature within the detrapping process are shown in **Figure 3**a ($\Delta\alpha = \alpha_T - \alpha_0$). Here, α_T is the absorption coefficient at certain temperature (T) and α_0 is the absorption coefficient of the already detrapped sample at 650K. In this measurement, Xe lamp act as the charging light source as well. The in-situ transmittance spectra of the YAGG: Pr^{3+} sample during charging process and heating process are shown in Figure S7a and S7b (Supporting Information), respectively. For the charging process, the absorption coefficient was plotted as a function of charging time (Figure S7c, Supporting Information). After the absorption intensity became saturated during Xe lamp charging at room temperature, the sample was heated from 300K to 650K with a heating rate of 5K min^{-1}. The integrated absorption intensity deconvoluted from $\Delta\alpha$ spectra per 10K monitoring photochromic center at 321 and 478 nm were plotted as a function of temperature in Figure 3b. With the rise in temperature, the absorption intensities of two photochromic centers decrease gradually. However, the absorption of photochromic center at 478 nm almost disappeared when the temperature reaches above 510K, while the absorption of the photochromic center at 321 nm can remain until the temperature upon 600K. Besides, the first derivative of absorption plot against the temperature is presented in Figure S8 (Supporting Information). The inconsistent response against temperature arising from two photochromic centers indicates that two photochromic centers have different trap depths. The photochromic center at 321 nm corresponds to much deeper traps compared with another photochromic center. All the results confirmed that two photochromic centers have distinct detrapping behavior during the heating process. Thus, it can be concluded that the UV charging induced coloration can be derived from the formation of two photochromic centers, which can serve as relatively shallow and deep electron traps to store excitation energy during the charging process. Besides, when the color sample was heated up to 300°C, the trapped electrons can acquire enough energy

to escape from the traps and return to their initial stages, and the sample recovers to greenish transparent state.

It is known that photochromism is generally a reversible photoinduced transformation process by light irradiation or thermal stimulus. To study the reversibility of coloration and decoloration, in-line transmittance at 550 nm of the sample after alternative 254 nm UV light irradiation for 5 min at room temperature and heating at 300°C for several cycles are shown in Figure 3c. The sample exhibits robust fatigue resistance due to reversible photoinduced transformation process by UV light charging and thermal stimulus, which enhances the great potential of the YAGG: Pr^{3+} transparent ceramic for optical storage applications.

2.3 Long PersL Properties of YAGG: Pr^{3+} Transparent Ceramic

PersL materials are typically excited by high-energy UV light and emit visible and infrared afterglow. In the present work, long PersL of YAGG: Pr^{3+} transparent ceramic can be obtained by either UV light charging or blue light through the up-conversion charging process. After ceasing the 280/450 nm irradiation, the corresponding PersL spectra of the as-made sample at room temperature were recorded as shown in **Figure 4**a and b. The normalized spectra were recorded at 10s after shutting off the light source as presented in Figure 4c, and the insert photograph exhibits the sample with red PersL after UV irradiation for 5 min. PersL spectra under UV/blue light irradiation show the characteristic emission peaks of Pr^{3+} ions, and strong red PersL in 600-650 nm region because of the Pr^{3+}: $^1D_2 \rightarrow {}^3H_4$ transition. Additionally, the PersL spectrum under 450 nm irradiation exhibits a nearly identical shape as the PersL spectrum ($\lambda_{irrad.} = 280$ nm), indicating that the trapping process of PersL is realized via up-conversion charging. The schematic energy level diagram in **Figure 7** elucidates the mechanism of PersL via up-conversion charging process. By intense blue light excitaion, the system was first excited to $^3P_2$ level of Pr^{3+} ion and fast non-radiative relaxation to the $^3P_0$ excited state. The high pumping intensity of the laser diode enables the population of the $^3P_0$ excited state to be high enough to produce substantial excited state absorption. Such an excited $^3P_0$ state can

successively absorb another blue light photon to further pump the system to the delocalized state, and fulfill the up-conversion charging process. Subsequently, the electrons could be detrapped by thermal energy at ambient temperature and cause the PersL. However, it should be noted that few or no PersL in the UV range under both two different excitation light source. The reason of lack of UV PersL is mainly due to the photochromic center and the electron traps in the sample. As mentioned above, the absorption band of the photochromic center was found to be broad in the UV/visible range after charging. There may be two possibilities: one is the energy transfer from Pr^{3+} 5d level to the photochromic center due to the overlapping with 5d-4f emission and photochromic absorption; the other is the electron transfer process from 5d level to electron traps through the tunnelling process.[37]

A key parameter evaluating the PersL performance is the luminance duration time after ceasing the light source at room temperature. The PersL decay curve (in luminance units) in the Log-Log scale of the sample by UV/450 nm irradiation for 5 min, is shown in Figure 4d. The strong red PersL of the sample can be detectable by human eyes in a dark room under either UV or blue light irradiation. The two PersL decay curves visualize identical slopes which correspond to the PersL decay rate demonstrating the same detrapping process via different charging light sources. The luminance duration time can last for approximately 27483s (7.63h) before it drops to 0.32 mcd m^{-2} (a value commonly used in the safety signage industry, defined as about 100 times higher than the limit of human eye sensitivity) by 5 min UV light charging.
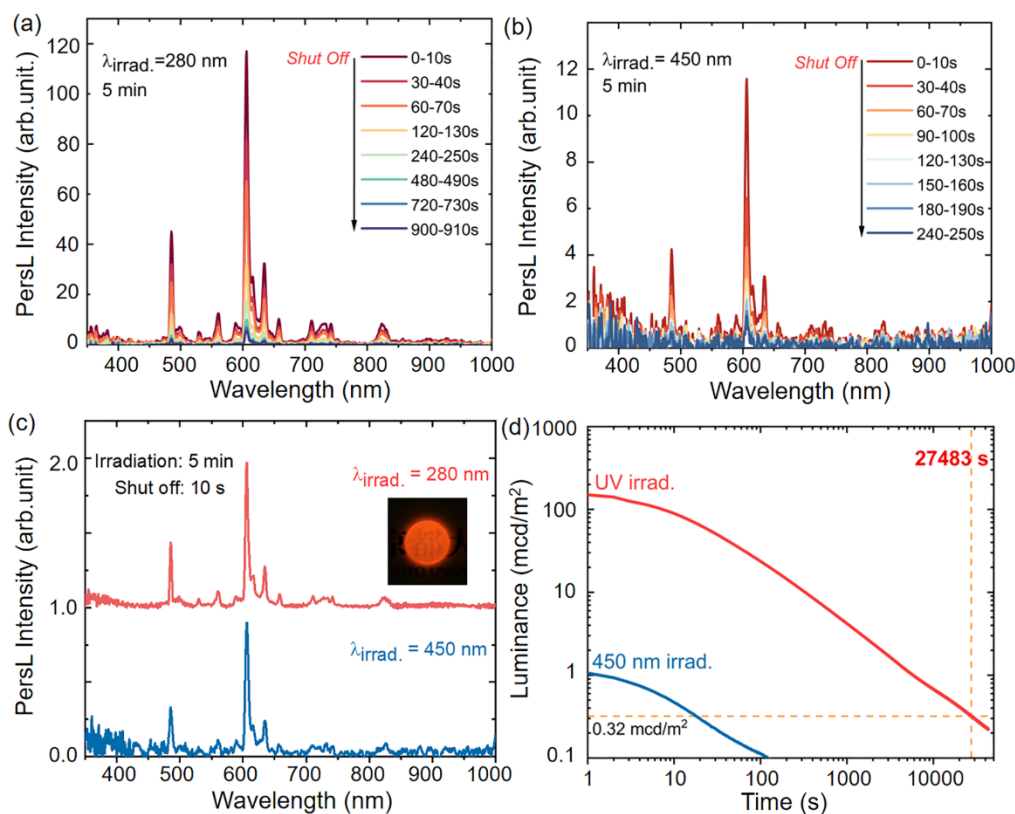
Figure 4. a) PersL spectra after ceasing light source under 280 nm and b) 450 nm light irradiation for 5 min. c) Normalized PersL spectra at 10s after ceasing the light source. d) Luminance decay curves after UV/blue light irradiation for 5 minutes.

It is recognized that both photochromism and PersL are owing to the presence of defects in inorganic materials. Thermoluminescence (TL) is caused by the thermally detrapping of carriers that were previously trapped by defects followed by recombination on a luminescent center. TL is extremely sensitive to defects in the material and can therefore be a powerful tool to investigate the trap depth which is determined by the energy difference between the energy level of the trap and the conduction band.[38] Thus, knowing the trap depth is crucial to understand the mechanism of PersL. By measuring the TL intensity as a function of temperature at a constant heating rate, the TL glow curve can be obtained. The thermal quenching of Pr^{3+} 4f-4f luminescence was firstly measured by temperature dependence of PL intensity (Figure S9, Supporting Information). The PL intensity for the Pr^{3+} 4f-4f luminescence becomes 63.3% at high temperature (600K) with respect to the PL intensity at 300K. **Figure 5**a presents the TL glow curve of the YAGG: Pr^{3+} transparent ceramic with a heating rate of 10 K min^{-1} (calibrated

by the temperature dependence of PL intensity). The TL glow curve shows two intense peaks located at 387 K and 522 K (fitted by Gussian function). Two peaks originated from the intrinsic defects corresponding to the signature of electrons released from the traps. The trap depth can be estimated by the well-known first-order kinetics presented by Randall and Wilkins: [39]

$$\frac{\beta\varepsilon}{kT_m^2} = s \times \exp\left(-\frac{\varepsilon}{kT_m}\right) \tag{4}$$

where β is the heating rate (K min^{-1}), k is the Boltzman constant (eV K^{-1}), ε is the trap depth, s is the frequency factor (s^{-1}) and T_m is the TL glow curve peak temperature (K). Because the frequency factor depends on the host material other than the dopants, the frequency factor of YAGG: Pr^{3+} transparent ceramic can be assumed to be 1.0×10^{13} s^{-1} of the YAGG (x = 3.0): Ce^{3+}-Cr^{3+} sample.[31] Then the trap depth values of two peaks can be estimated from the TL glow curve at 10K min^{-1} heating rate, which are 1.15 and 1.54eV. Additionally, it is considered that the TL glow curve correlates with the temperature dependence of absorption intensity of two photochromic centers.[40] The first temperature derivative of $\Delta\alpha$ could be proportional to the detrapped electrons with increasing the temperature. Figure S8 (Supporting Information) presents that the first derivative of $\Delta\alpha$ of two photochromic centers are similar to TL glow curve. The results further proved that the electron traps of TL and photochromism are identical. Additionally, the trap depths in the phosphor are much larger than the empirical value of 0.5-0.8 eV reported in conventional room temperature PersL phosphors,[27] which suggests that the YAGG: Pr^{3+} transparent ceramic is suitable for the optical storage application because of a large number of deep traps to store the recorded data. The TL 2D contour plot of the YAGG: Pr^{3+} transparent ceramic as a function of wavelength and temperature is also essential to further clarify the contributing emission bands to the TL glow curve, as shown in Figure 5b. The photograph of the sample in the upper-right presents bright reddish TL under 387K. From the contour plot of the sample recorded by the Si CCD, TL emission spectra under 387 and 522K are composed of Pr^{3+} luminescence center, the peak at 607 nm originates from the Pr^{3+}: $^1D_2 \rightarrow$

$^3H_4$ emission, and the weak Pr^{3+}: $^3P_0 \to {}^3H_4$ luminescence at around 487 nm is also observed.

Both two TL emission spectra show good agreement with the PersL spectra in Figure 4, indicating that the TL and PersL are related to the electron detrapped from the trap centers.
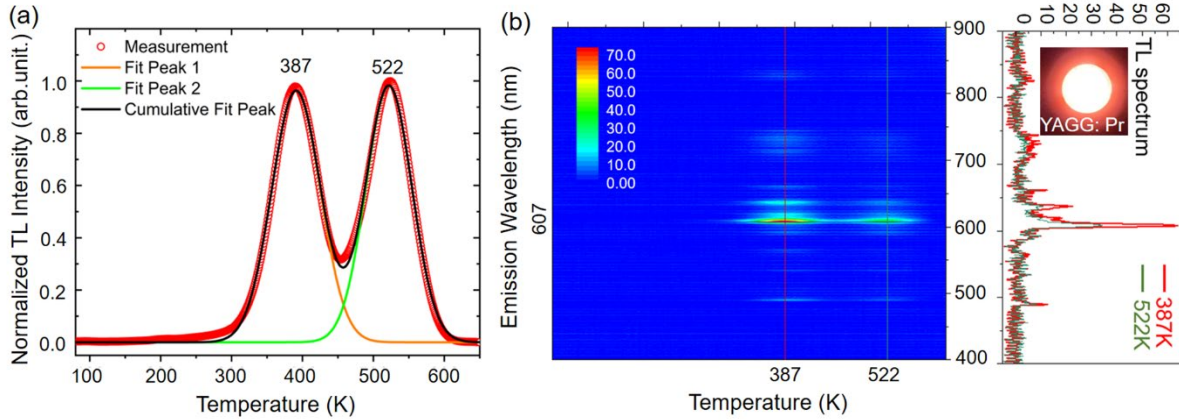

Figure 5. a) TL glow curve of the YAGG: Pr^{3+} transparent ceramic with a heating rate of 10 K min^{-1}. The sample was irradiated by UV light (250 to 380 nm) from a mercury lamp for 5 min. b) Wavelength−temperature (λ-T) 2D TL contour mapping of the YAGG: Pr^{3+} transparent ceramic. The right projection shows the TL emission spectrum at 387 and 522K.

2.4 Electron Spin Resonance Study of Trap Centers

Electron spin resonance (ESR) is a common method to identify the trap centers for many photochromic and PersL materials.[41] ESR is based on the fact that atoms with an odd number of electrons exhibit characteristic magnetic properties, and it has proven to be a useful tool for identifying defect structures and doping ions. Since the YAGG: Pr^{3+} transparent ceramic was sintered in vacuum atmosphere, we assumed that oxygen vacancies can act as trap centers since oxygen vacancies $V_O^{\cdot\cdot}$ usually exist in the phosphors synthesized under vacuum or reducing atmosphere. As proof, we measured the ESR spectra before and after UV irradiation (**Figure 6**a). In the case of the as-made sample without UV irradiation, the ESR spectrum shows no signal. However, the ESR spectrum shows a signal in the 322-357 mT magnetic field range after UV irradiation for 5min, corresponding to g-factors in the 2.05 to 1.85 range. The ESR signal shows an asymmetric line which can be fitted by Gaussian function in Figure 6b with two main peak signals of $g_1 = 1.998$ and $g_2 = 1.930$. Two g values suggest that at least two kinds of electron traps exist. The g value mainly originated from ionized oxygen vacancy in garnet.[42]

It is probably attributed to the different magnetically inequivalent positions of the oxygen vacancies in the garnet lattice. Similar results caused by oxygen vacancies have been reported previously.[43] These magnetically inequivalent positions correspond to distinct directions of the Al(IV)–V_O–Al(VI) chains (paths) in the unit cell. Moreover, it is commonly accepted that the oxygen vacancy-based photochromic centers are typical defects in aluminum garnets, because of the inert or even vacuum atmosphere used during sintering. Defects of oxygen vacancies in the sample binding free electrons lead to a significant ESR signal after UV light irradiation. Therefore, it is proved that large numbers of oxygen defects $V_O^{\cdot\cdot}$ were introduced in the YAGG: Pr^{3+} transparent ceramic, which is major for the photochromism and PersL properties.
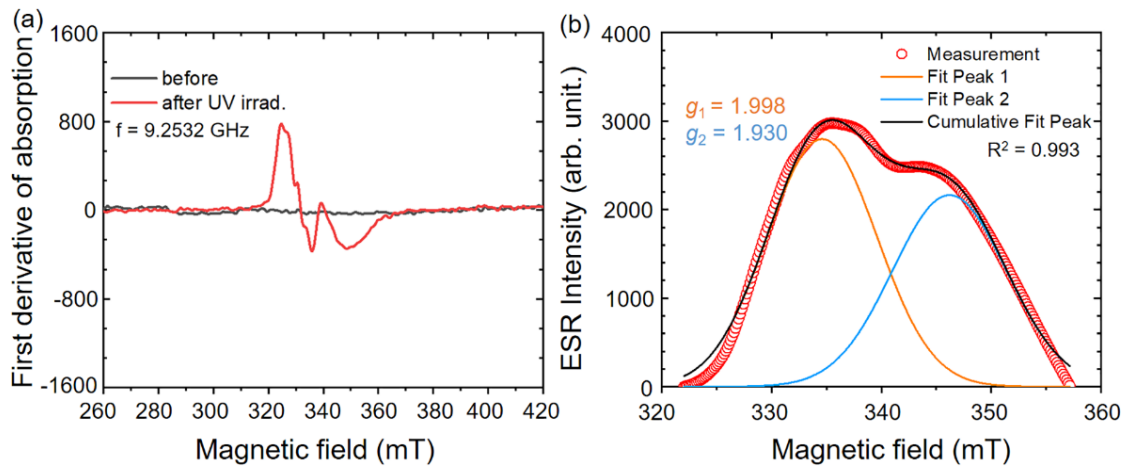

Figure 6. a) ESR spectra of YAGG: Pr^{3+} transparent ceramic before (black) and after 5 min UV irradiation (red) in the X band at room temperature. b) Decomposition of the ESR line after UV irradiation into two Gaussian components demonstrating anisotropy of the g factor.

3. Photochromism and Persistent Luminescence Mechanism

Based on the results above, we may elucidate the photochromism and PersL mechanism by using the VRBE energy diagram of YAGG along with the charging and detrapping process as illustrated in Figure 7. Firstly, the 4f ground state electrons of Pr^{3+} are excited into the conduction band under UV/blue light irradiation through the 5d levels, followed by being trapped subsequently by the electron trap centers of intrinsic defects-oxygen vacancies $V_O^{\cdot\cdot}$. The reversible conversion between $V_O^{\cdot\cdot}$ and $V_O^{\cdot}$ by trapping and releasing an electron corresponding

to both the shallow traps and deep traps causes photochromism. Besides, the trapped electrons also can be detrapped slowly from shallow traps to recombine center without external excitation at room temperature owing to thermal vibration, which is responsible for the persistent luminescence. The creation of trapping centers may be caused in the following way. Oxygen vacancies $V_O^{\cdot\cdot}$ usually exist in the phosphors synthesized under vacuum or reducing atmosphere. The presence of intrinsic defects-oxygen vacancies for photochromism causes the reversible conversions between $V_O^{\cdot\cdot}$ and $V_O^{\cdot}$ by trapping and releasing an electron. In addition, Ga volatilization can be easily formed during the high temperature sintering process. We propose that V_{Ga}''' could be responsible for the negative effective charge defects, which are generated for the charge compensation.
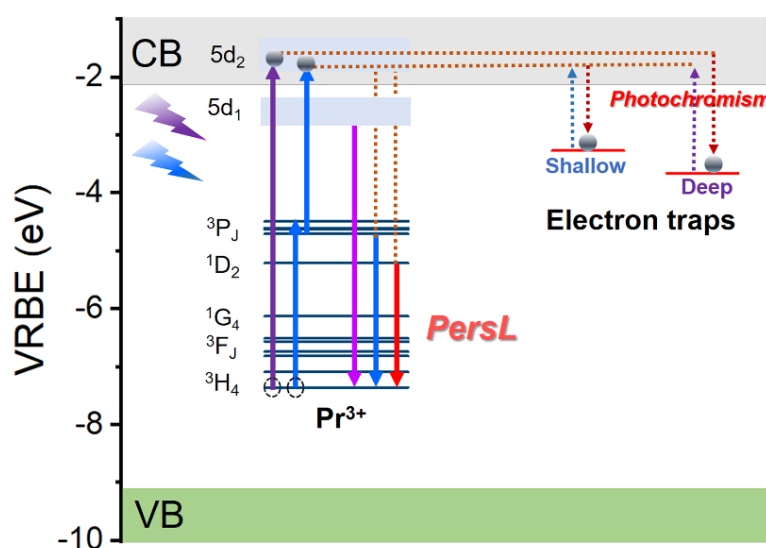

Figure 7. VRBE energy levels and schematic illustration of charging and detrapping electrons in YAGG: Pr[3+] transparent ceramic.

4. Toward Optical Storage Applications

The optical storage applications based on photochromic and PersL phosphors were extensively reported.[44] The schematic illustration of the write-in and read-out, erasing and rewriting by altering between UV/blue light irradiation and thermal bleaching at 300℃ is shown in **Figure 8**a. As an example, the information display in YAGG: Pr[3+] transparent ceramic is presented in Figure 7b. The sample covered by mask A was irradiated using a 254 nm mercury lamp. After

the information write-in by 5 min UV irradiation, the reddish patterns of the mask were displayed based on the photochromic behavior in the light room. Benefit from the high transmittance of the sample, reddish patterns not only on the surface but inside the body of the sample after irradiation. For the dark field, the write-in information can be read out by TL because of deep trap depth, as discussed above. The forming information can be bleached upon thermal stimulus. The recovered sample also can be reused many times with different masks (Mask B and Mask C), which enhances the potential applicability for the optical storage field. Notably, the information can remain for more than 3 weeks as shown in Figure 2. Furthermore, optical information write-in can also be realized by up-conversion charging using a 450 nm laser. One can see remarkable signal augment with increasing laser irradiation times in Figure 8b. As a consequence, the better optical data retention ability and optional irradiation light source by either UV or blue light endow the YAGG: Pr^{3+} transparent ceramic with potential feasibility in various optical storage applications.
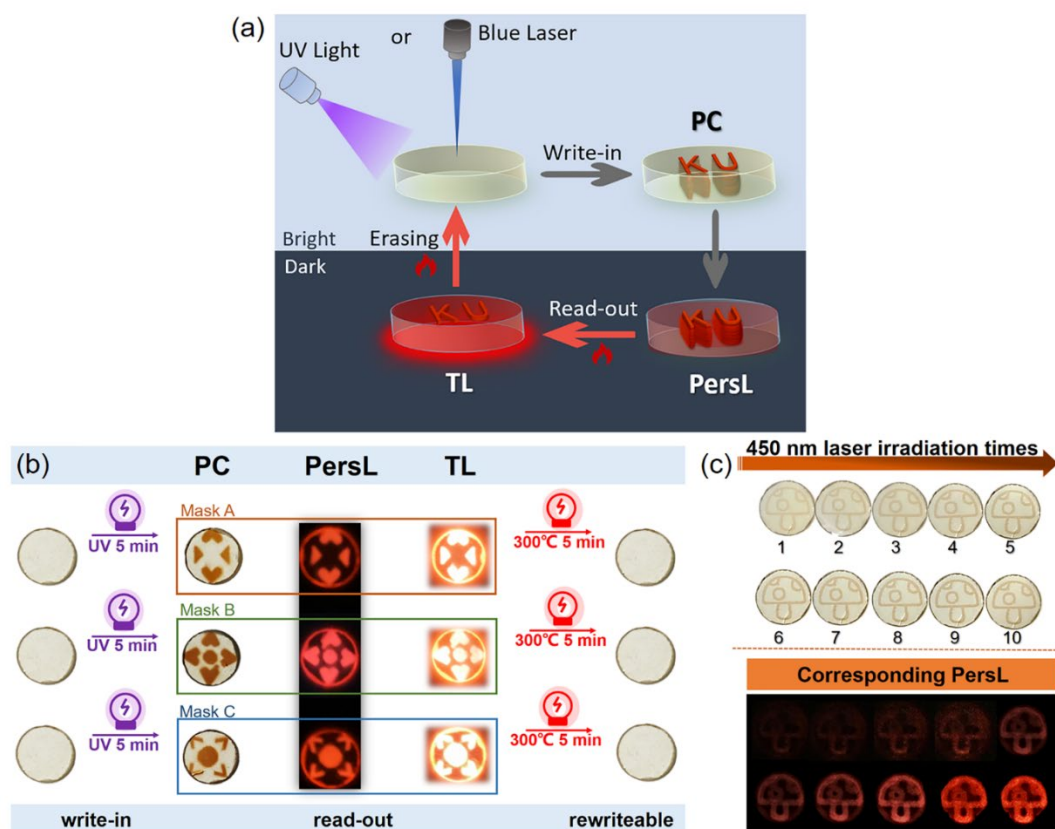
Figure 8. a) Schematic illustration of the write-in and read-out of optical information. b) Optical information display of write-in, read-out and bleaching based on photochromism (PC) and PersL in YAGG: Pr^{3+} transparent ceramic by altering between 254 nm irradiation and 300°C thermal stimulus. c) Demonstration experiment for optical information storage in the YAGG: Pr^{3+} transparent ceramic by increasing 450 nm laser irradiation times, showing the mode of up-conversion write-in and read-out with corresponding PersL 30s after ceasing the light source.

5. Conclusion

In summary, a multifunctional transparent ceramic phosphor by doping Pr^{3+} into $Y_3Al_2Ga_3O_{12}$, aiming at obtaining novel optical information storage material, has been successfully synthesized for the first time. The phosphor exhibits both photochromism and strong red persistent luminescence after several minutes UV light charging or blue light up-conversion charging. The reversibility of greenish-reddish color change by alternating UV/blue light irradiation and thermal stimulus, demostrates excellent fatigue resistance. In the case of UV irradiation, the luminance can last for 27483s (7.63h) before it drops to 0.32 mcd/m^2, additionally, the reddish color can remain for more than three weeks. Two trap centers of intrinsic defects-oxygen vacancies $V_O^{\ddot{}}$ with different trap depths were deeply studied with the assistance of in-situ time dependence and temperature dependence of $\Delta\alpha$, TL, and ESR. By using the VRBE energy diagram, the mechanism of photochromism and PersL has been elucidated and discussed comprehensively. The study of YAGG: Pr^{3+} transparent ceramic gives researchers an insight into the nature of traps involved in photochromism and PersL, and offers an opportunity for designing novel multifunctional materials applied in the optical information storage fields.

6. Experimental Section

Sample Preparation: Polycrystalline ceramics of $Y_3Al_2Ga_3O_{12}$ and $Y_3Al_2Ga_3O_{12}$: Pr^{3+} (0.1%) were synthesized using solid-state reactions. The chemicals Y_2O_3 (99.99%), Al_2O_3 (99.99%), Ga_2O_3 (99.99%), and Pr_6O_{11} (99.99%) were used as the starting materials. The powders were mixed by ball milling (Fritsch, Premium Line P-7) with ethanol. The obtained slurry was dried in an oven for 20 hours to remove the ethanol solvent and pulverized. The powders were pressed

at 50 MPa into pellets (Φ=20 mm) and then sintered at 1650°C for 12 h under a vacuum atmosphere. The obtained transparent ceramics were double-surface polished simultaneously by using a copper plate and diamond slurry, and the final thickness was 1.3±0.1 mm.

Characterization: The crystalline phases of transparent ceramic samples were identified as garnet crystals using an X-ray diffraction (XRD) equipment (Ultima IV, Rigaku). The as-made non-doped and Pr^{3+}-doped samples were confirmed to be single phase without any impurities (Figure S10, Supporting Information). Surface microstructural properties and the distribution of elements in the YAGG: Pr^{3+} transparent ceramic was characterized using scanning electron microscopy (SEM, SU8220, HITACHI, Japan) with an X-ray energy detector (EDX, HORIBA, Japan) system. No other impurity elements in the preparation process of the transparent ceramic in this experiment. The sample presents a fully dense microstructure and homogenous elements distribution (Figure S11, Supporting Information).

Optical Measurements: Photoluminescence excitation (PLE) spectra were measured with a setup consisting of a Xe lamp (OPM2-502XQ, Ushio Inc.), double monochromators (SP-300i, Acton Research Corp.), and a photomultiplier tube (R3896, Hamamatsu Photonics). The PLE spectra were calibrated by the spectrum of the Xe lamp (excitation light source) detected by a Si standard photodiode (S1337-1010BQ, Bunkoukeiki Co. Ltd.). Photoluminescence (PL) and PersL spectra of the samples were measured at 300K by a Si CCD spectrometer (QE65-Pro, Ocean Optics) and calibrated by a standard halogen lamp. An optical parametric oscillator laser (NT342B-20-SH/SF, Ekspla) was used as the excitation source for PL and PersL measurements. For the up-conversion investigation, the sample set in a cryostat (Helitran LT3, Advanced Research Systems) at 80 K was pumped by a 450 nm CW laser. The ceramic sample was also firstly heated up to 750K to empty the trap and cooled down to 80K. The in-line transmittance spectra were measured by a UV-vis-NIR spectrometer (UV-3600, Shimadzu). For the in-situ transmittance spectra, the measurement setup was composed of a Xe lamp (MAX-302, Asahi Spectra Co., Ltd, Japan) that acted as the excitation source as well, a CCD spectrometer

(QE65Pro, Ocean Optics) and thermal stage for the heating process. UV lamp (SP-9, Ushio) was used as the excitation source for thermoluminescence (TL) two-dimensional (2D) plot measurements. The transparent ceramic sample was set in a cryostat (VPF-800, Janis) to control temperatures and firstly heated up to 750K to empty the trap and cooled down to 80K. The sample was irradiated by UV light at 80 K for 5 min, then heated up to 650 K at a rate of 10 K min^{-1} after ceasing the irradiation. The TL signals were recorded by a PMT detector (R11041, Hamamatsu Photonics & Co. Ltd.,). The same Si CCD spectrometer was operated simultaneously with the TL measurement to monitor the TL emission spectra at different temperatures. The PersL decay curves of the sample were obtained at room temperature with the same PMT detector as in the TL measurement. The sample was excited for 5 min by the UV lamp (SP-9, Ushio) at UV range of 250-350 nm and by a 450 nm CW laser for up-conversion charging. Then, the decay curves were converted to luminance (in the unit of mcd m^{-2}) by PersL Intensity. The PersL spectra of the sample after ceasing the light source were detected by a calibrated CCD spectrometer (GlacierX BTRANSPARENT CERAMIC112E, B&W Tek). Electron spin resonance (ESR) spectra were measured using JEOL type JES-RE2X X-band spectrometer at room temperature before and after 254 nm UV lamp irradiation for 5min. Before irradiation, the sample was detrapped under 350°C for 5 min.

Optical Information Write-in and Read-out: The multifunctional phosphor was covered by Mask A, Mask B, and Mask C with specific patterns, and irradiated by UV light (254 nm mercury lamp) for 5 min. The desired information was recorded after ceasing the UV light and removing the mask. The recorded data read-out can be realized by TL at target temperature. Additionally, blue light laser (MASTER 2, NEJE) can be used as write-in light source for optical data storage on the transparent ceramic as well. The mushroom patterns were engraved under blue light excitation with different irradiation times.

Supporting Information

Supporting Information is available from the Wiley Online Library or from the author.

References

[1] a) M. Hilbert, P. Lopez, *Science* **2011**, *332*, 60; b) M. Gu, X. Li, Y. Cao, *Light-Sci. Appl.* **2014**, *3*, 11.

[2] a) D. A. Parthenopoulos, P. M. Rentzepis, *Science* **1989**, *245*, 843; b) J. Zhang, M. Gecevicius, M. Beresna, P. G. Kazansky, *Phys. Rev. Lett.* **2014**, *112*, 5; c) M. Gu, Q. Zhang, S. Lamon, *Nat. Rev. Mater.* **2016**, *1*, 14; d) D. Liu, L. Yuan, Y. Jin, H. Wu, Y. Lv, G. Xiong, G. Ju, L. Chen, S. Yang, Y. Hu, *ACS Appl. Mater. Interfaces* **2019**, *11*, 35023; e) Z. Hu, X. Huang, Z. Yang, J. Qiu, Z. Song, J. Zhang, G. Dong, *Light-Sci. Appl.* **2021**, *10*, 9.

[3] a) H. Durr, in *Photochromism: Molecules And Systems*, Vol. 40 (Eds: H. Durr, H. Bonauslaurent), Elsevier Science Bv, Amsterdam **1990**, 1; b) M. Irie, T. Fulcaminato, K. Matsuda, S. Kobatake, *Chem. Rev.* **2014**, *114*, 12174.

[4] a) Y. L. Han, M. Hamada, I. Y. Chang, K. Hyeon-Deuk, Y. Kobori, Y. Kobayashi, *J. Am. Chem. Soc.* **2021**, *143*, 2239; b) K. Fujita, S. Hatano, D. Kato, J. Abe, *Org. Lett.* **2008**, *10*, 3105; c) J. Harada, R. Nakajima, K. Ogawa, *J. Am. Chem. Soc.* **2008**, *130*, 7085.

[5] G. Jaume, D. Velasco. *Beilstein J. Org. Chem.* **2012**, *8*, 1003.

[6] L. A. Frolova, A. A. Rezvanova, B. S. Lukyanov, N. A. Sanina, P. A. Troshin and S. M. Aldoshin. *J. Mater. Chem. C* **2015**, *3*, 11675.

[7] C. M. Sousa, J. Berthet, S. Delbaere, A. Polonia, P. J. Coelho. *J. Org. Chem.* **2017**, *82*, 12028.

[8] A. Spangenberg, R. Métivier, J. Gonzalez, K. Nakatani, P. Yu, M. Giraud, A. Léaustic, R. Guillot, T. Uwada, T. Asahi. *Adv. Mater.* **2009**, *21*, 309.

24

[9] J. Wei, X. Jiao, T. Wang, D. Chen, *J. Mater. Chem. C* **2015**, *3*, 7597.

[10] D. M. Tobaldi, S. G. Leonardi, R. C. Pullar, M. P. Seabra, G. Neri, J. A. Labrincha, *J. Mater. Chem. A* **2016**, *4*, 9600.

[11] J. N. Yao, K. Hashimoto, A. Fujishima, *Nature* **1992**, *355*, 624.

[12] Q. Zhang, H. Sun, H. Li, X. Wang, X. Hao, J. Song, S. An, *Chem. Commun.* **2015**, *51*, 16316.

[13] K. Li, L. Luo, Y. Zhang, W. Li, Y. Hou, *ACS Appl. Mater. Interfaces* **2018**, *10*, 41525.

[14] H. Wang, J. Lin, B. Deng, T. Lin, C. Lin, Y. Cheng, X. Wu, X. Zheng, X. Yu, *J. Mater. Chem. C* **2020**, *8*, 2343.

[15] M. Akiyama, H. Yamada, K. Sakai, *J. Ceram. Soc. Jpn*. **2011**, *119*, 105

[16] X. Bai, Z. Yang, Y. Zhan, Z. Hu, Y. Ren, M. Li, Z. Xu, A. Ullah, I. Khan, J. Qiu, Z. Song, B. Liu, Y. Wang, *ACS Appl. Mater. Interfaces* **2020**, *12*, 21936.

[17] Y. Zhang, L. Luo, K. Li, W. Li, Y. Hou, *J. Mater. Chem. C* **2018**, *6*, 13148.

[18] a) J. Holsa, *Electrochem. Soc. Interface* **2009**, *18*, 42; b) Y. Zhuang, Y. Lv, L. Wang, W. Chen, T. L. Zhou, T. Takeda, N. Hirosaki, R. J. Xie *ACS Appl. Mater. Interfaces* **2018**, *10*, 1854; c) D. Poelman, D. Van der Heggen, J. R. Du, E. Cosaert, P. F. Smet, *J. Appl. Phys.* **2020**, *128*, 13.

[19] T. Matsuzawa, Y. Aoki, N. Takeuchi, Y. Murayama, *J. Electrochem. Soc*. **1996**, *143*, 2670.

[20] a) P. F. Smet, N. Avci, K. Van den Eeckhout, D. Poelman, *Opt. Mater. Express* **2012**, 2, 1306; b) J. Ueda, T. Shinoda, S. Tanabe, *Opt. Mater. Express* **2013**, *3*, 787; c) P. Dorenbos, *Phys. Status Solidi B-Basic Solid State Phys*. **2005**, *242*, R7.

[21] Y. Wang, Z. Wang, *J. Rare Earths* **2006**, *24*, 25.

[22] D. Jia, W. Jia, D. R. Evans, W. M. Dennis, H. Liu, J. Zhu, W. M. Yen, *J. Appl. Phys*. **2000**, *88*, 3402.

[23] T. Aitasalo, A. Hietikko, D. Hreniak, J. Holsa, M. Lastusaari, J. Niittykoski, W. Strek, *J. Alloy. Compd*. **2008**, *451*, 229.

[24] K. Van den Eeckhout, P. F. Smet, D. Poelman, *J. Lumines*. **2009**, *129*, 1140.

[25] J. Ueda, S. Tanabe, K. Takahashi, T. Takeda, N. Hirosaki, *Bull. Chem. Soc. Jpn*. **2018**, *91*, 173.

[26] B. Wang, H. Lin, J. Xu, H. Chen, Z. Lin, F. Huang, Y. Wang, *Inorg. Chem*. **2015**, *54*, 11299.

[27] a) Y. Chen, F. Liu, Y. Liang, X. Wang, J. Bi, X. J. Wang, Z. Pan, *J. Mater. Chem. C* **2018**, 6, 8003; b) J. Xu, S. Tanabe, *J. Lumines*. **2019**, *205*, 581.

[28] a) F. Liu, Y. Liang, Z. Pan, *Phys. Rev. Lett*. **2014**, *113*, 5; b) F. Liu, Y. Chen, Y. Liang, Z. Pan, *Opt. Lett*. **2016**, *41*, 954.

[29] a) J. Xu, J. Ueda, K. Kuroishi, S. Tanabe, *Scr. Mater*. **2015**, *102*, 47; b) J. Ueda, S. Miyano, S. Tanabe, *ACS Appl. Mater. Interfaces* **2018**, *10*, 20652.

[30] a) K. Asami, J. Ueda, S. Tanabe, *J. Lumines*. **2019**, *207*, 246; b) V. Castaing, L. Giordano, C. Richard, D. Gourier, M. Allix, B. Viana, *J. Phys. Chem. C* **2021**, *125*, 10110.

[31] a) P. Dorenbos, *J. Mater. Chem*. **2012**, *22*, 22344; b) P. Dorenbos, *J. Lumines*. **2013**, *134*, 310; c) J. Xu, J. Ueda, S. Tanabe, *J. Mater. Chem. C* **2016**, *4*, 4380; d) J. Ueda, P. Dorenbos, A. J. J. Bos, K. Kuroishi, S. Tanabe, *J. Mater. Chem. C* **2015**, *3*, 5642. e) J. Ueda, *Bull. Chem. Soc. Jpn.* **2021**, *94*, 2807.

[32] a) S. Yan, Q. Gao, X. Zhao, A. Wang, Y. Liu, J. Zhang, X. J. Wang, F. Liu, *J. Lumines*. **2020**, *226*, 117427; b) S. Yan, F. Liu, J. Zhang, X. J. Wang, Y. Liu, *Phys. Rev. Appl*. **2020**, *13*, 8.

[33] a) J. B. Gruber, M. E. Hills, R. M. Macfarlane, C. A. Morrison, G. A. Turner, *Chemical Physics* **1989**, *134*, 241; b) E. Cavalli, L. Esposito, M. Bettinelli, A. Speghini, K. V. Ivanovskikh, R. B. Hughes-Currie, M. De Jong, *Materials Research Express* **2014**, *1*, 045903; c) A. Lukowiak, R. J. Wiglusz, M. Maczka, P. Gluchowski, W. Strek, *Chem. Phys. Lett*. **2010**, *494*, 279.

[34] a) C. D. Donega, A. Meijerink, G. Blasse, *J. Phys. Chem. Solids* **1995**, *56*, 673; b) R. Naccache, F. Vetrone, A. Speghini, M. Bettinelli, J. A. Capobianco, *J. Phys. Chem. C* **2008**, 112, 7750.

[35] G. Özen, O. Forte, B. Di Bartolo, *J. Appl. Phys*. **2005**, *97*, 013510.

[36] H. Zhao, Y. Cun, X. Bai, D. Xiao, J. Qiu, Z. Song, J. Liao, Z. Yang, *ACS Energy Lett.* **2022**, *7*, 2060.

[36] a) J. Botterman, J. J. Joos, P. F. Smet. *Phys. Rev. B* **2014**, *90*, 085147. b) C. Tydtgat, K. W. Meert, D. Poelman, P. F. Smet. *Opt. Mater. Express* **2016**, *6*, 844.

[37] P, Avouris, T. N. Morgan, *J. Chem. Phys.* **1981**, 74, 4347.

[38] a) J. R. Du, K. L, R. V. D, D. Poelman, H. L, *Adv. Opt. Mater*. **2022**, *10*, 2101714; b) J. Ueda, *Bull. Chem. Soc. Jpn*. **2021**, *94*, 2807; c) A. J. J. Bos, *Radiat. Meas*. **2007**, *41*, S45; d) Y. Zhuang, L. Wang, Y. Lv, T. L. Zhou, R. J. Xie, *Adv. Funct. Mater*. **2018**, *28*, 1705769.

[39] a) J. T. Randall, M. H. F. Wilkins, *Proc. R. Soc. A Math. Phys. Eng. Sci.* **1945**, *184*, 390, 12; b) J. T. Randall, M. H. F. Wilkins, *Proc. R. Soc. A Math. Phys. Eng. Sci.* **1945**, *184*, 366.

[40] J. Ueda, A. Hashimoto, S. Tanabe, *J. Phys. Chem. C* **2019**, *123*, 29946.

[41] a) Y. Ren, Z. Yang, M. Li, J. R, J. Zhao, J. Qiu, Z. Song, D. Zhou, *Adv. Opt. Mater.* **2019**, *7*, 1900213; b) Y. Han, M. Hamada, I. Y. Chang, H. D. Kim, Y. Kobori, Y. Kobayashi, *J. Am. Chem. Soc.* **2021**, *143*, 2239.

[42] a) K. Mori, *physica status solidi (a)* **1977**, *42*, 375; b) M. Nikl, A. Vedda, M. Fasoli, I. Fontana, V. V. Laguta, E. Mihokova, J. Pejchal, J. Rosa, K. Nejezchleb, *Phys. Rev. B* **2007**, *76*, 8.

[43] a) M. Nikl, V. Laguta, A. Vedda, *Physica status solidi (b)* **2008**, *245*, 1701; b) V. Laguta, M. Buryi, P. Arhipov, O. Sidletskiy, O. Laguta, M. Brik, M. Nikl, *Phys. Rev. B* **2020**, *101*, 024106.

[44] a) Z. Hu, X. Huang, Z. Yang, J. Qiu, Z. Song, J. Zhang, G. Dong, *Light Sci. Appl.* **2021**, *10*, 140. b) Z. Yang, J. Hu, L. I. D. J. Martin, D. Van der Heggen, D. Poelman. *J. Mater. Chem. C* **2021**, *9*, 14012.

Table of Contents

The developed multifunctional Pr^{3+}-doped $Y_3Al_2Ga_3O_{12}$ transparent ceramic for optical storage application, exhibiting both photochromism and red persistent luminescence with long luminance duration time of more than 7 h, has been successfully prepared for the first time. The multifunctional properties can be achieved by either UV light or blue light up-conversion excitation.

Qiping Du*, Jumpei Ueda*, Ruilin Zheng, and Setsuhisa Tanabe

Photochromism and Long Persistent Luminescence in Pr^{3+}-Doped Garnet Transparent Ceramic via Ultraviolet or Blue Light Up-conversion Charging

ToC figure